



## OPEN ACCESS

EDITED BY  
Gabriele Multhoff,  
Technical University of Munich,  
Germany

REVIEWED BY  
Xiuping Yu,  
Louisiana State University Health  
Shreveport, United States  
Xiaohong Li,  
University of Toledo, United States

\*CORRESPONDENCE  
Xin Lu  
xlu@nd.edu

SPECIALTY SECTION  
This article was submitted to  
Cancer Immunity  
and Immunotherapy,  
a section of the journal  
Frontiers in Immunology

RECEIVED 27 July 2022

ACCEPTED 04 October 2022

PUBLISHED 20 October 2022

CITATION  
Rahmy S, Mishra SJ, Murphy S,  
Blagg BSJ and Lu X (2022) Hsp90 $\beta$   
inhibition upregulates interferon  
response and enhances immune  
checkpoint blockade therapy in  
murine tumors.  
*Front. Immunol.* 13:1005045.  
doi: 10.3389/fimmu.2022.1005045

COPYRIGHT  
© 2022 Rahmy, Mishra, Murphy, Blagg  
and Lu. This is an open-access article  
distributed under the terms of the  
[Creative Commons Attribution License  
\(CC BY\)](https://creativecommons.org/licenses/by/4.0/). The use, distribution or  
reproduction in other forums is  
permitted, provided the original  
author(s) and the copyright owner(s)  
are credited and that the original  
publication in this journal is cited, in  
accordance with accepted academic  
practice. No use, distribution or  
reproduction is permitted which does  
not comply with these terms.

# Hsp90 $\beta$ inhibition upregulates interferon response and enhances immune checkpoint blockade therapy in murine tumors

Sharif Rahmy<sup>1,2</sup>, Sanket J. Mishra<sup>3</sup>, Sean Murphy<sup>1</sup>,  
Brian S. J. Blagg<sup>3</sup> and Xin Lu<sup>1,2,4\*</sup>

<sup>1</sup>Department of Biological Sciences, Boler-Parseghian Center for Rare and Neglected Diseases, Harper Cancer Research Institute, University of Notre Dame, Notre Dame, IN, United States,

<sup>2</sup>Integrated Biomedical Sciences Graduate Program, University of Notre Dame, Notre Dame, IN, United States, <sup>3</sup>Department of Chemistry and Biochemistry, Warren Family Research Center for Drug Discovery and Development, University of Notre Dame, Notre Dame, IN, United States,

<sup>4</sup>Tumor Microenvironment and Metastasis Program, Indiana University Melvin and Bren Simon Comprehensive Cancer Center, Indianapolis, IN, United States

Response resistance to the immune checkpoint blockade (ICB) immunotherapy remains a major clinical challenge that may be overcome through the rational combination of ICB and specific targeted therapeutics. One emerging combination strategy is based on sensitizing ICB-refractory tumors with antagonists of 90kD heat shock protein (Hsp90) that target all four isoforms. However, pan-Hsp90 inhibitors are limited by the modest efficacy, on-target and off-tumor toxicities, and induction of the heat shock response (HSR) that overrides the effect of Hsp90 inhibition. Recently, we developed Hsp90 $\beta$ -selective inhibitors that were cytotoxic to cancer cells but did not induce HSR *in vitro*. Here, we report that the Hsp90 $\beta$  inhibitor NDNB1182 downregulated CDK4 (an Hsp90 $\beta$ -dependent client protein) and induced the expression of endogenous retroviral elements and interferon-stimulated genes. In syngeneic mouse models of prostate cancer and breast cancer, NDNB1182 significantly augmented the efficacy of ICB therapy. Furthermore, NDNB1182 showed superior tolerability to the pan-Hsp90 inhibitor Ganetespib in mice. Our findings provide evidence that Hsp90 $\beta$  inhibition is a potentially effective and safe regimen to combine with ICB to treat immunotherapy-refractory solid tumors.

## KEYWORDS

heat shock protein 90 (hsp90), isoform-selective inhibitor, immune checkpoint blockade (ICB), prostate cancer, breast cancer, CDK4/6, interferon response, endogenous retrovirus

## Introduction

Novel immunotherapies have revolutionized the treatment of cancer patients in recent years. The broadest impact comes from immune checkpoint blockade (ICB) that reinvigorates anti-tumor cytotoxic T lymphocytes (CTLs) using antibodies against CTLA4 or PD1/PD-L1 and generates therapeutic responses across a variety of cancer types (1). However, some solid tumor types remain largely resistant to ICB therapy, including breast cancer and prostate cancer which represent the first and third most frequently diagnosed malignancies worldwide, respectively (2). Advanced prostate cancer (metastatic and castration-resistant) shows overwhelming *de novo* resistance to anti-CTLA4 or anti-PD1 therapies (3–6). When ipilimumab and nivolumab were combined in a preliminary phase II clinical trial (CheckMate 650), improved objective response rates were reported (25% and 10% for pre- and post-chemotherapy), yet inadequate response rate and strong adverse effect remain frustrating (7). For metastatic triple-negative breast cancer, two ICB drugs, atezolizumab and pembrolizumab, in combination with chemotherapy, have been approved by the FDA to treat PD-L1<sup>+</sup> cases (8, 9). However, the majority of the patients remain nonresponsive to ICB therapy. In order to bring broad benefits to patients with advanced prostate cancer and breast cancer, therapeutic approaches to overcome the resistance and sensitize the disease to ICB are urgently needed.

The 90kD heat shock protein (Hsp90) family functions as an evolutionarily conserved molecular chaperone to regulate protein homeostasis under physiological and stress conditions (10–13). Hsp90 family consists of four members: Hsp90 $\alpha$  (inducible) and Hsp90 $\beta$  (constitutive) in the cytoplasm, glucose-regulated protein 94 (Grp94) in endoplasmic reticulum, and tumor necrosis factor receptor-associated protein-1 (Trap1) in mitochondria. Hsp90 proteins are responsible for the proper folding, disaggregation and intracellular trafficking of over 400 client proteins, including protein kinases, steroid hormone receptors, transcription factors, E3 ubiquitin ligases and more. Many of these clients control the hallmarks of cancer, therefore inhibition of Hsp90 may offer a unique benefit of co-targeting many oncogenic pathways (13). Various reports suggest that mutated and overexpressed oncoproteins rely more on the Hsp90 chaperone activity for proper folding, thus neoplastic cells may be more dependent on the function of Hsp90 chaperone for survival and proliferation than normal cells are, which could create a therapeutic window (14–17).

Many cell types express Hsp90 on the cell surface or secrete Hsp90 into the extracellular space (18, 19), and often Hsp90 expressed on the cell surface is more abundant in cancer cells than normal cells (20). Tumor cells appear to be more sensitive to Hsp90 inhibition, because the Hsp90 complex in cancer cells is distinct from normal cells with its higher affinity binding state

(14). Moreover, in approximately 50% of cancers especially those fueled by MYC, Hsp90 acts as a nucleating site to form functionally integrated complexes termed ‘epichaperome’, which render tumor cells more sensitive to Hsp90 inhibitors (Hsp90i) (17). Lastly, Hsp90i preferentially accumulate in tumor cells as compared with normal cells (21–23). Therefore, Hsp90 is an attractive target for developing drugs to treat malignancies, including prostate cancer and breast cancer (24, 25).

Following the discovery of natural product inhibitors of Hsp90, geldanamycin (26) and radicicol (27), avid investment in the design, synthesis and evaluation of drug-like Hsp90i ensued (16, 28). So far, 18 small molecule drugs as pan-Hsp90 inhibitors (pan-Hsp90i) have entered clinical trials, but none has demonstrated satisfactory benefit-risk profile to be approved by the Food and Drug Administration (FDA) (29, 30). Pan-Hsp90i target the N-terminal domain (NTD) and bind competitively to the ATP binding site of all four Hsp90 isoforms. Challenges with current Hsp90i include limited efficacy, dose-limiting toxicities (DLTs), and various on-target and off-tumor toxicities. A major cause of the limited efficacy and DLTs is the induction of the pro-survival heat shock response (HSR) by pan-Hsp90 inhibition, because pan-Hsp90i trigger dissociation of heat shock factor 1 (Hsf1) from Hsp90 complex and Hsf1 subsequently enters nucleus and activates the transcription of Hsp27, Hsp40, Hsp70 and Hsp90 (31, 32), which counteracts the effect from the inhibitor. On the other hand, Hsp90i-associated hepatic, cardio and ocular toxicities may result from the disruption of clients. For example, the cardiac potassium channel human ether-a-go-go related gene (hERG) depends on Hsp90 for functional maturation, thus Hsp90i can cause deleterious effects on the hERG-related membrane potential (33). Interestingly, hERG is solely dependent on Hsp90 $\alpha$  (34), suggesting that inhibition of Hsp90 $\alpha$  (but not other isoforms) is likely to account more for the cardio and ocular toxicities. Moreover, Hsp90 $\alpha$  and Hsp90 $\beta$  govern clientele and exert biological functions in non-redundant manners despite highly similar structures (35, 36), emphasizing the value of developing isoform-selective inhibitors. Using a structure-based molecular design and optimization approach, Blagg and colleagues developed various Grp94 inhibitors (37–40), Hsp90 $\alpha$  inhibitors (Hsp90 $\alpha$ -i) (41, 42), and Hsp90 $\beta$  inhibitors (Hsp90 $\beta$ -i) (43, 44). Among them, Hsp90 $\beta$ -i induce degradation of Hsp90 $\beta$ -dependent clients without concomitant degradation of Hsp90 $\alpha$  clients or induction of the HSR (43, 44). Therefore, Hsp90 $\beta$ -i may overcome the obstacles encountered by pan-Hsp90i that have struggled in clinical trials.

Emerging evidence shows the involvement of Hsp90 in tumor immunity and the potential of enhancing immunotherapy with Hsp90i, although the mechanisms remain inadequately characterized and all these studies used pan-Hsp90i. For example, Ganetespiib induced type I interferon response genes, such as interferon-induced protein with tetratricopeptide repeats (IFIT), through an unknown

mechanism and promoted tumor cell killing by autologous T cells *in vitro* and anti-CTLA4 immunotherapy in mouse model of colorectal cancer (45). In addition, Ganetespib and 17-AAG decreased PD-L1 transcription through destabilizing Hsp90 clients MYC and STAT3 in monocytes and tumor cells at the sub-cytotoxic concentration, and Ganetespib diminished PD-L1 level on MC38 tumor cells *in vivo* (46). It is not yet explored whether isoform-selective Hsp90i, especially Hsp90 $\beta$ -i, can sensitize prostate cancer and breast cancer to immunotherapy, which is the central question for the current study to address.

## Results

### HSP90 $\beta$ -selective inhibitor NDNB1182 inhibits cell proliferation

We first conducted *in silico* analysis to support the proposition of inhibiting Hsp90 $\beta$  to enhance ICB therapy. From a phase 2 clinical trial of ipilimumab (anti-CTLA4) in 30 patients with metastatic castration-resistant prostate cancer (47), we retrieved the expression values of *HSP90AB1* (encoding Hsp90 $\beta$ ) from the published RNA-seq data of the patient samples in the study (n=18) and separated the cohort to HSP90AB1<sup>high</sup> and HSP90AB1<sup>low</sup> groups. We compared the two groups for PSA progression free survival (PFS) and overall survival (OS). HSP90AB1<sup>high</sup> group showed significantly worse outcome than the HSP90AB1<sup>low</sup> group under ipilimumab therapy (Figure 1A). Next, we noticed that the KMplot tool recently gathered the survival data for patients across various cancer types treated with ICB therapies (48), so we used KMplot to compare the OS of HSP90AB1<sup>high</sup> and HSP90AB1<sup>low</sup> patients for either anti-PD1 treatment or anti-PD-L1 treatment. In both regimens, patients with HSP90AB1<sup>high</sup> tumors showed significantly shorter OS (Figure 1B).

The Blagg laboratory recently reported the structure-based rational development of the 2H-isoquinolin-1-one based series of Hsp90 $\beta$ -i (44). To enhance the solubility of these Hsp90 $\beta$ -i compounds for *in vivo* application, Blagg's group replaced the solvent exposed fragment (cyclohexanolamine) to reduce intermolecular pi-stacking, and synthesized the newest Hsp90 $\beta$ -i, NDNB1182 (Figure 1C) (Mishra et al, manuscript under preparation). Like other 2H-isoquinolin-1-one series of Hsp90 $\beta$ -i, NDNB1182 was evaluated for the binding affinities against the four Hsp90 isoforms by measuring the ability to competitively displace FITC-labeled geldanamycin (a pan-Hsp90i) in a fluorescence polarization (FP) assay (44, 49). NDNB1182 exhibited improved selectivity (over 150-fold) for the Hsp90 $\beta$  isoform over the highly identical Hsp90 $\alpha$  isoform (Figure 1C). While pan-HSP90i luminespib reduced expression of the HSP90 $\alpha$ -selective client protein Src (42, 50), NDNB1182 did not alter Src levels (Figure 1D). The purity of the compound was confirmed to be >95% by high-performance liquid

chromatography (HPLC) (Figure 1E). We performed the resazurin assay to evaluate the cytotoxicity of NDNB1182 against murine colorectal cancer cell line MC38, murine prostate cancer cell lines Pten-CaP8 and RM1, and murine Lewis lung carcinoma LLC. The IC50 values for all the lines fell below 100nM and did not show significant differences among the lines (P = 0.0889, Figure 1F). As comparison, the effect of NDNB1182 was tested on two normal cell types, mouse prostate primary epithelial cells (grown from the dissociated prostate glands of wild type C57BL/6 mice) and the mouse fibroblast cell line L cells (ATCC, CRL-2648). IC50 of NDNB1182 was 430nM for normal prostate cells and 1255nM for L cells (Figure 1G), which were significantly higher than the IC50 values of the four mouse prostate cancer cell lines. Next, we plotted HSP90AB1 expression levels in various human prostate lineage cell lines at the Depmap portal. The result showed that various prostate cancer tissue-derived cell lines (MDAPCA2B, VCAP, NCIH660, LNCAP, 22Rv1, PC3) expressed HSP90AB1 at higher levels than the normal-like or ectopically transformed prostate cell lines (PRECLH, WPE1NA22, P4E6, SHMAC4, SHMAC5) (Figure 1H). Overall, these results support that Hsp90 $\beta$  is a promising target for prostate cancer and suggest that NDNB1182 selectively targets Hsp90 $\beta$ .

### NDNB1182 upregulates IFIT and endogenous retroviral element expression

The pan-Hsp90i Ganetespib was reported to induce IFIT1 expression at 125nM and higher (45). To examine whether isoform-selective Hsp90 $\alpha$ -i or Hsp90 $\beta$ -i has this activity, we treated MC38 with Ganetespib, Hsp90 $\alpha$ -i 12h (42) and NDNB1182 for 6 hours. Hsp90 $\alpha$  inhibition induced no increase in *Ifit1* expression, whilst Ganetespib and NDNB1182 both significantly increased *Ifit1* expression with NDNB1182 inducing *Ifit1* by a higher magnitude (Figure 2A). We further confirmed the dose-dependent induction of IFIT1 expression by NDNB1182 in human prostate cancer cell line DU145 (Figure 2B).

Mbofung et al. did not identify the mechanism for Ganetespib to induce interferon-stimulated genes (ISGs), which is addressed in our study. We previously showed that Hsp90 $\beta$ -i compounds led to degradation of Hsp90 $\beta$ -dependent clients including CDK4 but did not trigger the undesired HSR such as HSF1 upregulation (43, 44). NDNB1182 was confirmed to induce a dose-dependent decline of CDK4 expression, but no increase of HSF1 (Figure 2C). Our result reinforced that CDK4/6 are Hsp90 $\beta$ -selective clients (51, 52). Interestingly, CDK4/6 inhibition was shown to reduce the expression of DNMT1 (encoding DNA methyltransferase 1), an E2F target gene, resulting in hypomethylation of the genome and activation of the expression of endogenous retroviral (ERV) elements and

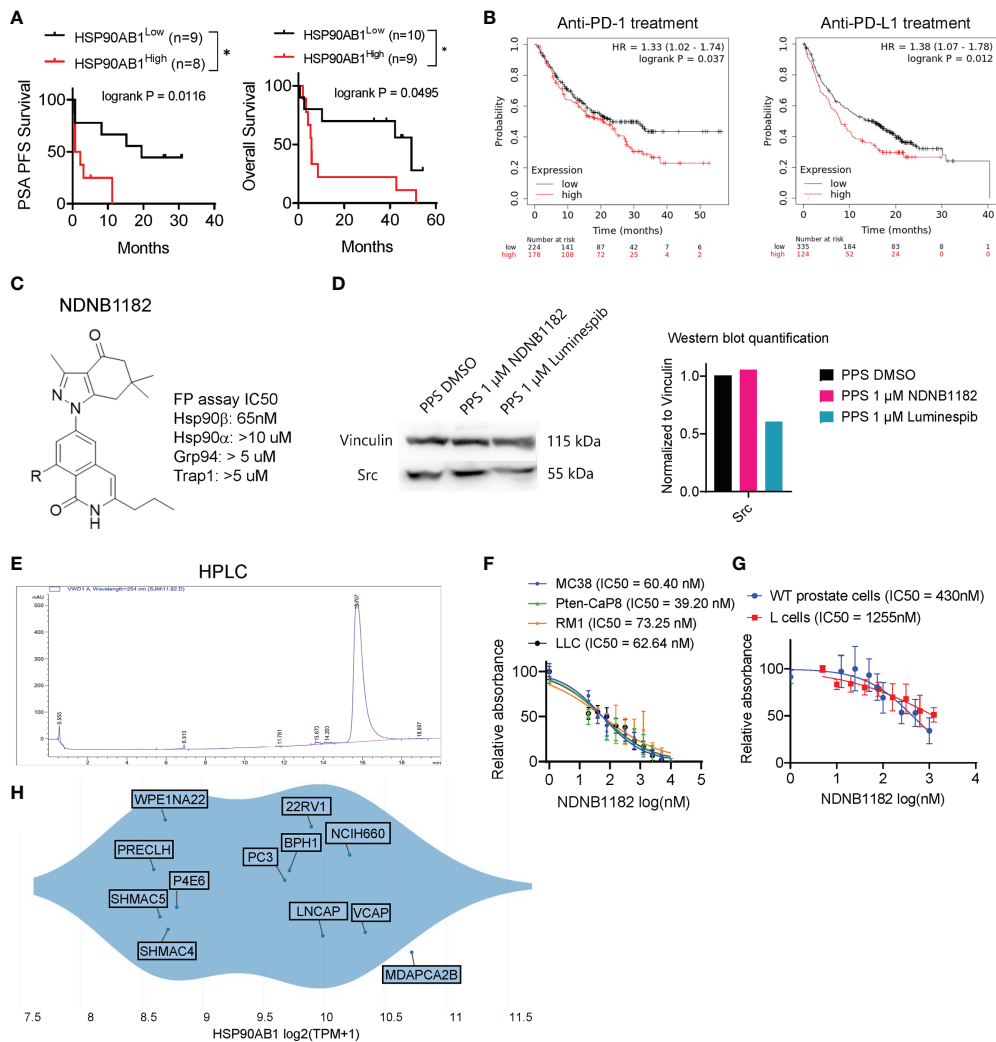
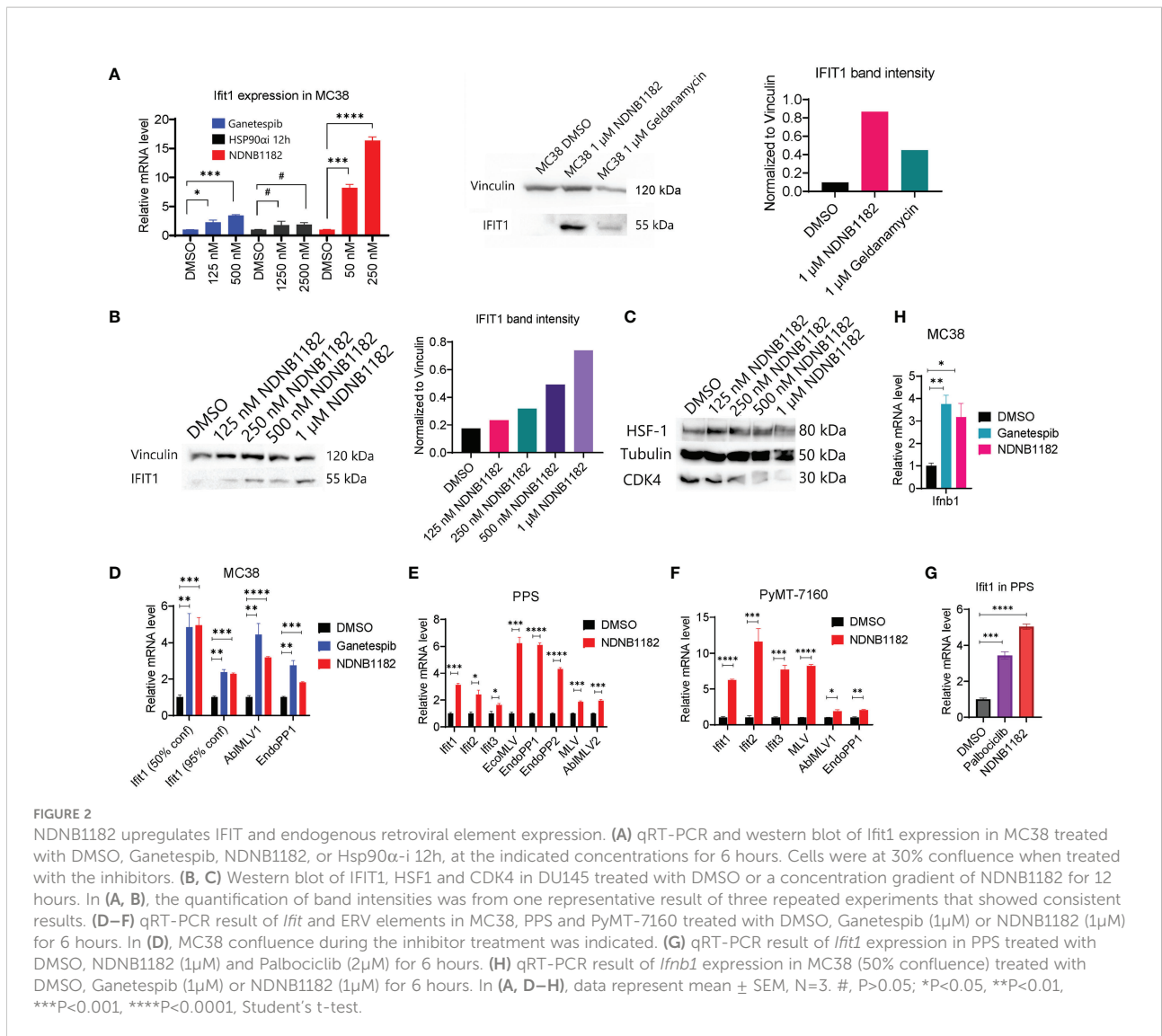


**FIGURE 1**  
Hsp90β-selective inhibitor NDNB1182. **(A)** Association of high *HSP90AB1* expression with worse PSA progression free survival (PFS) and overall survival, with data extracted from the database of a phase 2 clinical trial of ipilimumab in metastatic castration-resistant prostate cancer \* $P < 0.05$ , log rank test between the two cohorts (47). **(B)** Association of high *HSP90AB1* expression with worse overall survival for anti-PD-1 or anti-PD-L1 treatment with data from multiple clinical studies, drawn with KMplot. **(C)** The generic structure of NDNB1182 and IC50 values against Hsp90 isoforms determined using fluorescence polarization (FP) assay. **(D)** Western blot of Src in mouse prostate cancer cell line PPS treated with DMSO, NDNB1182 or luminespib for 12 hours, with the semi-quantitative result presented on the right. **(E)** HPLC result confirming the high purity of NDNB1182. **(F)** Dose-response curves and IC50 values of NDNB1182 on four cancer cell lines. Nonlinear regression modeling with log (inhibitor) and normalized response of variable slopes was conducted in Graphpad Prism. **(G)** Dose-response curves and IC50 values of NDNB1182 on primary prostate epithelial cells grown from wild type C57BL/6 mice and the mouse fibroblast cell line L cells. **(H)** *HSP90AB1* transcript levels for prostate-lineage cell lines in the Depmap database portal with the plot generated by Depmap.

ISGs to enhance tumor antigen presentation and ultimately anti-tumor immunity (53). Taking these together, we hypothesized that NDNB1182 could achieve an equivalent effect as CDK4/6 inhibitor (like Palbociclib) to stimulate ERV and anti-viral ISG expression. To test this, we treated MC38 with Ganetespib and NDNB1182 and examined the expression of a list of murine ERV elements (54). Both inhibitors stimulated the levels of *Ifit1* and ERV genes *AbiMLV1* and *EndoPP1* (Figure 2D).

Interestingly, we observed that lower confluence of MC38 cells corresponded to higher *Ifit1* induction by both Hsp90 inhibitors (Figures 2A, D). This observation may be related to the DNA methylation dynamics during cell cycle (see Discussion). We expanded the treatment and detection to more syngeneic cell lines: the prostate cancer cell line PPS that we developed from the *PB-Cre<sup>+</sup> Pten<sup>L/L</sup> p53<sup>L/L</sup> Smad4<sup>L/L</sup>* transgenic mouse model (55), and a mammary cancer cell line PyMT-7160 that we



established in this study from the MMTV-PyMT (mouse mammary tumor virus promoter driven polyoma middle T-antigen) transgenic mice with autochthonous mammary adenocarcinoma (56). In both cell lines, NDNB1182 induced the expression of *Ifit* genes and various ERV elements (AbiMLV1/2, EcoMLV, EndoPP1/2, MLV), although the exact fold changes differed (Figures 2E, F). Furthermore, both NDNB1182 and Palbociclib induced *Ifit1* expression in PPS (Figure 2G). *Ifnb1* (encoding interferon  $\beta$ 1, a major type I interferon) was upregulated significantly in MC38 cells treated with Ganetespiib and NDNB1182 (Figure 2H). These results demonstrate that NDNB1182, by inhibiting Hsp90 $\beta$  but not other isoforms, can downregulate CDK4/6 expression, activate ERV elements and stimulate the interferon response in cancer cells. This trait prompted us to test whether NDNB1182 could enhance ICB therapy.

### NDNB1182 enhanced ICB efficacy in the PPS syngeneic prostate cancer model

We tested the anti-tumor effect of NDNB1182 in two prostate cancer syngeneic models, Myc-CaP and PPS. Myc-CaP was derived from c-myc transgenic mice in the FVB/N background (57) and responded poorly to ICB therapy (58). We confirmed that Myc-CaP failed to shrink under anti-PD1 plus anti-CTLA4 ICB treatment (Figure 3A). In this model, neither NDNB1182 (dosed at 50mg/kg, daily) nor Ganetespiib (dosed at 25mg/kg, daily) had a significant impact on tumor growth (Figure 3B). Nevertheless, this model provided promising results for the toxicity profile of NDNB1182, because in the same experiment while Ganetespiib showed significant toxicity leading to 80% (4 out of 5) mortality within 13 days of treatment, mice treated with NDNB1182 at two-fold of the dose showed no significant change of survival (Figure 3C).

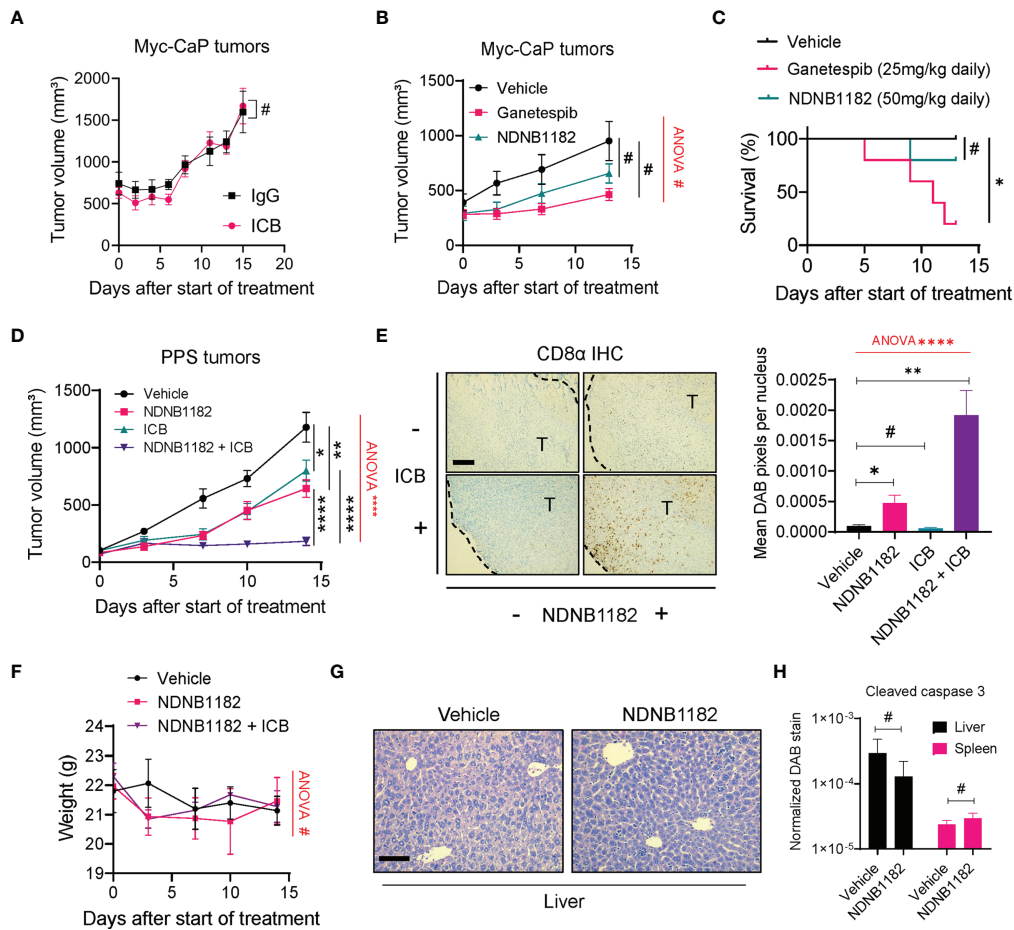


FIGURE 3

NDNB1182 enhanced ICB efficacy in the PPS syngeneic prostate cancer model. (A) Growth curves of Myc-CaP tumors treated with isotype IgG or ICB (anti-PD1 plus anti-CTLA4) administered intraperitoneally (i.p.) at 10mg/kg, twice/week. N=9/group. (B) Growth curves of Myc-CaP tumors treated with vehicle, GanetespiB (25mg/kg, i.p. daily) or NDNB1182 (50mg/kg, i.p. daily). N=10 tumors/group at the start of the treatment. (C) Survival curves for mice bearing Myc-CaP tumors and treated with vehicle, GanetespiB or NDNB1182. N=5/group. (D) Growth curves of PPS tumors treated with vehicle control (N=6), NDNB1182 (50mg/kg, i.p. daily; N=6), ICB (anti-PD1 plus anti-CTLA4, 10mg/kg, i.p., twice/week; N=10), or concurrent NDNB1182 plus ICB (N=8). In (A, B, D), the randomized groups on day 0 of the treatment showed no significant difference based on statistical tests (for (A) two groups at day 0, P=0.8238 based on Mann Whitney test; for (B) three groups at day 0, P=0.4265 based on ANOVA test; for (D) four groups at day 0, P= 0.5561 based on ANOVA test). (E) Representative images and quantification results for CD8α immunohistochemistry on PPS tumors treated with the four regimens. The tumor regions (“T”) and the margin contours are denoted. N=5 for each condition. Image analysis and quantification was performed with ImageJ following a published protocol (59), where DAB signals were normalized to the number of nuclei present in the images. Scale bar 200µm. (F) Body weight changes of mice treated with vehicle, NDNB1182, or NDNB1182 plus ICB. (G) Representative H&E staining images of liver from vehicle-treated and NDNB1182-treated mice. Scale bar 50µm. (H) Quantification results for cleaved caspase 3 immunohistochemistry on liver and spleen tissues from vehicle-treated and NDNB1182-treated mice. In (A–H), data represent mean ± SEM. #P>0.05; \*P<0.05, \*\*P<0.01, \*\*\*\*P<0.0001, Student’s t-test. In (B, D–F), one-way ANOVA test result was shown in red (#P>0.05; \*\*\*\*P<0.0001). In (C), #P>0.05; \*P<0.05, logrank test.

PPS tumors grown in C57BL/6 background responded partially to ICB monotherapy (60). We treated PPS-carrying animals with vehicle control, NDNB1182, ICB (anti-PD1 + anti-CTLA4), or combination of NDNB1182 and ICB. Therapy with NDNB1182 or ICB each showed partial response, but the combination achieved remarkably enhanced efficacy (Figure 3D). Immunohistochemistry (IHC) staining of CD8α demonstrated that NDNB1182 alone induced a moderate

increase of CD8<sup>+</sup> T cell infiltration to the tumors, ICB alone had no effect, but the NDNB1182 plus ICB combination dramatically augmented the infiltration of CD8<sup>+</sup> T cells (Figure 3E). Importantly, the animal body weight was not affected by NDNB1182 or NDNB1182 plus ICB treatments, showing low toxicity by NDNB1182 monotherapy or the combination treatment (Figure 3F). Furthermore, vehicle and NDNB1182 treated mice showed no discernable histological

differences in the liver (Figure 3G) or the spleen (data not shown). NDNB1182 also caused no increase in apoptosis (as indicated by positive cleaved caspase 3 staining) in the liver or spleen (Figure 3H). These results provide further support for the safety of NDNB1182 at the dosage used.

The results from Myc-CaP and PPS models connect the anti-tumor activity of NDNB1182 with the ICB response of the models and illustrate the potential of enhancing ICB therapy with Hsp90β inhibition.

### NDNB1182 enhanced ICB therapy in the PyMT-7160 syngeneic mammary tumor model

To test the activity of NDNB1182 to enhance immunotherapy in another tumor type, we orthotopically injected FVB/N female mice with PyMT-7160 mammary cancer cells and implemented a similar design of single and combination treatments. NDNB1182 and ICB each had moderate impact on tumor growth, but the NDNB1182 and ICB combination showed dramatic anti-tumor activity (Figure 4A). We dissociated the tumors at the endpoint

and quantified the CTLs (CD45<sup>+</sup> CD8<sup>+</sup>) and antigen-presenting dendritic cells (DCs, CD11c<sup>+</sup> MHC-II<sup>+</sup>) with flow cytometry. We quantified CD11c<sup>+</sup> MHC-II<sup>+</sup> DCs because these cells may play an important role in presenting the tumor antigens to activate the T cell immunity. Consistent with the anti-tumor efficacy, only the NDNB1182 plus ICB treatment stimulated the tumor infiltration of both CTLs (Figures 4B, C) and DCs (Figures 4D, E) significantly compared with the control. We further confirmed that tumors treated with ICB plus NDNB1182 expressed *Ifit* genes and ERV elements MLV and EcoMLV at the highest level compared with other treatment regimens (Figure 4F). These results support that the combination of Hsp90β inhibition and ICB offers the most potent control on breast cancer progression through ERV and interferon response activation and anti-tumor immunity reprogramming.

### Discussion

Most previous studies regarded Hsp90 chaperone as one machinery and inhibited Hsp90 activities in cancer models and clinical trials with pan-Hsp90i, which may largely account for

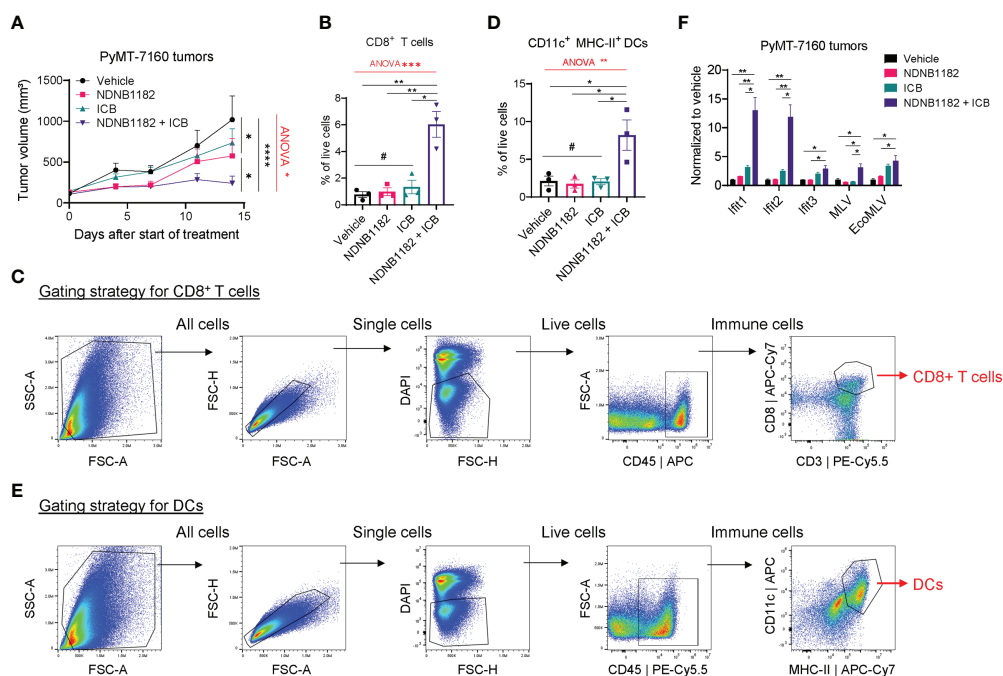


**FIGURE 4**  
 NDNB1182 enhanced ICB therapy in the PyMT-7160 syngeneic mammary tumor model. **(A)** Growth curves of PyMT-7160 tumors treated with vehicle control (N=8), NDNB1182 (50mg/kg, i.p. daily; N=10), ICB (anti-PD1 plus anti-CTLA4, 10mg/kg, i.p., twice/week; N=10), or concurrent NDNB1182 plus ICB (N=8). **(B, C)** Quantification results and gating strategy for tumor-infiltrating CD8<sup>+</sup> T cells in treated PyMT-7160 tumors. **(D, E)** Quantification results and gating strategy for tumor-infiltrating CD11c<sup>+</sup> MHC-II<sup>+</sup> dendritic cells (DCs) in treated PyMT-7160 tumors. **(F)** qRT-PCR result of *Ifit1/2/3* and two ERV elements for PyMT-7160 tumors treated with DMSO, NDNB1182, ICB, or NDNB1182 plus ICB (N=3/group). In **(A, B, D, F)**, data represent mean ± SEM. #P>0.05; \*P<0.05, \*\*P<0.01, \*\*\*\*P<0.0001, Student's t-test. In **(A, B, D)**, one-way ANOVA test result was shown in red (\*P<0.05, \*\*P<0.01, \*\*\*P<0.001).

the disappointing clinical performance of Hsp90 inhibition in cancer treatment so far. Because different Hsp90 isoforms have non-redundant functions executed by recognizing different sets of client proteins, targeting all isoforms is neither necessary nor beneficial. Here, we have challenged this paradigm by reporting, for the first time, the *in vivo* anti-tumor activity of Hsp90 $\beta$ -i and its potential as an immunotherapy sensitizer. Specifically, we made the following discoveries: (1) the new Hsp90 $\beta$ -i NDNB1182 demonstrated high selectivity toward Hsp90 $\beta$  over the other three Hsp90 isoforms and killed cancer cells at the lower 100nM IC50 level; (2) NDNB1182 induced the expression of various ERV elements and *Ifit* genes across different cancer cell lines; (3) NDNB1182 significantly augmented the efficacy from ICB therapy in the PPS prostate cancer and PyMT-7160 breast cancer models; (4) NDNB1182 displayed better tolerability than the pan-Hsp90i Ganetespiib and did not cause mouse body condition deterioration or rapid weight loss when dosed at tumor-restricting levels.

Pan-Hsp90i as cancer monotherapy in clinical trials has encountered many challenges of limited efficacy and DLTs, leading to the dampened interest in oncological targeting of Hsp90 (29, 30). For example, a phase II trial using AUY922 in patients with metastatic gastrointestinal stromal tumor only showed modest anti-tumor effect but caused significant ocular toxicity (61). However, recent publications linking Hsp90 function with cancer immune modulation and showing how Hsp90 inhibition may enhance cancer immunotherapy in preclinical models have revived the interest in the combination of Hsp90i and ICB in the clinic (62, 63). For example, there are at least two ongoing Phase I trials that combine Hsp90i (XL888, TAS-116) and anti-PD1 in advanced gastrointestinal cancers (NCT03095781, NCT04999761). Nevertheless, the on-target toxicities from inhibiting all Hsp90 isoforms remain a concern and may lead to the difficulty in dose management of the combination treatment (63). This reasoning further highlights the significance of developing isoform-selective Hsp90i, which may still achieve the desired efficacy by targeting the isoform-dependent oncoprotein clients while avoiding the toxicities associated with the disruption of other clients, such as Hsp90 $\alpha$  client hERG (34). To this end, we believe that Hsp90 $\beta$  emerges as the most promising isoform for the combinatorial targeting, because Hsp90 $\beta$ -i can induce degradation of Hsp90 $\beta$ -dependent clients that have well-established oncogenic functions (e.g. CDK4, CDK6, CXCR4, BRAF, HER2) without concomitant degradation of Hsp90 $\alpha$  clients or induction of the HSR (43, 44). Our study confirms that NDNB1182 is effective *in vitro* and *in vivo* without causing discernable toxicities in mice (by contrast, Ganetespiib was lethal even when administered at the half dose), electing NDNB1182 as a promising candidate for further preclinical validation and clinical development.

Our result showing that NDNB1182 activated the expression of ERV and IFIT genes is consistent with the previous finding with Ganetespiib (45), suggesting the inhibition of Hsp90 $\beta$

among all four isoforms likely contributed the most to the activity of Ganetespiib in the antiviral-like response in cancer cells. The CDK4 downregulation by NDNB1182 provides a logical mechanistic connection from Hsp90 $\beta$  inhibition to ERV and IFIT overexpression, because CDK4 is a client for Hsp90 $\beta$  and it is known that CDK4/6 inhibition can reactivate ERV expression and interferon response in cancer cells through downregulating DNMT1 expression and DNA methylation (53). CDK4/6 promotes Rb phosphorylation, leading to the release of E2F and subsequent transcriptional activation of E2F targets, including DNMT1. CDK4/6 inhibitors hinder the G1/S transition by inhibiting Rb phosphorylation and E2F release. Hsp90i may achieve the same effect by diminishing CDK4/6 protein level in the cells. Therefore, either by preventing Rb phosphorylation through CDK4/6 activity inhibition or by reducing the available pool of CDK4/6 through Hsp90 inhibition, the end result is a reduction in DNMT1 protein and subsequent DNA hypomethylation.

We noticed that the effect of NDNB1182 on *Ifit1* induction was inversely related to cell confluence during the inhibitor treatment (Figures 2A, D). Because DNMT1 as the maintenance methyltransferase is responsible for the preservation of 5-methylcytosine in the genome during DNA replication (64), we speculate that a less confluent cell culture has higher portion of dividing cells than a much more confluent cell culture, therefore, the effect of NDNB1182 on DNA hypomethylation and *Ifit1* upregulation became more manifested in less confluent cells. Further experiments will help verify this proposition. In addition, we notice that the specific ERV elements activated by NDNB1182 differed among the cell lines in our study, and it is probably caused by the distinct epigenetic status of these ERV elements in these cell lines. Nonetheless, all the cell lines showed IFIT upregulation, thus producing equivalent interferon response signaling output to cooperate with immune checkpoint inhibition to reinvigorate T cell immunity. Indeed, efficacious immunotherapy depends on a potentiated type I interferon response (65, 66).

There are a few limitations in our study. First, the *in vivo* results were generated only using syngeneic models. While these models have served well as preclinical platforms for immunotherapy discovery and development, other types of cancer models such as genetically engineered mouse models and humanized mouse models with patient-derived tumors and reconstituted human immune system will provide important confirmative evidence. Second, the immunotherapy-sensitizer activity of NDNB1182 was only tested together with ICB therapy. Other immunotherapy modalities such as oncolytic virus and CAR-T therapy may also benefit from the combination with Hsp90 $\beta$  inhibition, especially in solid tumors. Third, our study does not exclude other immune modulatory mechanisms by Hsp90 $\beta$  inhibition besides the CDK4-ERV-IFIT axis that may also contribute to the combinatorial efficacy from NDNB1182 plus ICB treatment,

which clearly warrants further investigations. Fourth, NDNB1182 was administered *via* intraperitoneal injection in our study, which would be inconvenient for the clinical application. Our teams are working on formulations that will allow oral delivery of NDNB1182 (or its improved analog). Lastly, given that hypomethylation and ERV may contribute to genomic instability in cancer (67, 68), the application of Hsp90 $\beta$  inhibition in clinical cancer therapy may not be suitable for certain patients (for example, young patients).

In conclusion, our results establish the preclinical evidence to support the rational combination of Hsp90 $\beta$  antagonists and immunotherapy in the treatment of intractable solid tumors, illuminating a clinical path for the better outcome of many cancer patients.

## Materials and methods

### Cell lines

Murine cell lines Pten-CaP8, RM1, LLC, and Myc-CaP and human cell line DU145 were purchased from ATCC and cultured in medium types recommended by ATCC. MC38 was purchased from kerafast and cultured in the recommended medium. PPS was developed from a spontaneous prostate tumor of *PB-Cre<sup>+</sup> Pten<sup>L/L</sup> p53<sup>L/L</sup> Smad4<sup>L/L</sup>* transgenic mice (55). PyMT-7160 was developed from a spontaneous mammary tumor of the FVB/N-Tg(MMTV-PyVT)634Mul/J mice (Jackson Laboratory, 002374). PPS and PyMT-7160 were cultured in DMEM (GE Healthcare, SH30243.FS) supplemented with 10% fetal bovine serum (GE Healthcare, SH30396.03) and 100U/ml penicillin-streptomycin (Caisson Labs, PSL01). All the cell lines were cultured at 37°C in a humidified incubator with 5% CO<sub>2</sub>. All cells were tested for mycoplasma-free status using a Mycoplasma Assay Kit (Agilent Technologies, 302109).

### Chemicals

Hsp90 $\alpha$ -i 12h (42) and Hsp90 $\beta$ -i NDNB1182 (Mishra et al, manuscript under preparation) were synthesized by the Blagg laboratory using the cited protocols. The identity of the chemicals was confirmed by high resolution mass spectrometry and nuclear magnetic resonance, while the purity of the compounds was confirmed to be >95% by high-performance liquid chromatography (HPLC). Ganetespib (MedChem Express, HY-15205) and Palbociclib (LC Laboratories, P-7788) were purchased.

### Mice

C57BL/6J males (Jackson Laboratory, 000664) and FVB/NJ males and females (Jackson Laboratory, 001800) were purchased at 5 weeks of age and used for experiments after one week of acclimation. All animals were maintained under pathogen-free conditions and cared for in accordance with the International Association for Assessment and Accreditation of Laboratory Animal Care policies and certification.

### Quantitative RT-PCR

RNA was isolated from cells and tissues using the EZ-10 Spin Column Total RNA Miniprep Kit (Bio Basic, BS1361) according to the manufacturer protocol. After RNA extraction, cDNA was synthesized using the All-in-one 5x RT MasterMix (ABM, G592). qPCR reactions were performed with the 2X SYBR Green Master mix (Bimake, B21203) and run on the CFX Connect Real-Time PCR Detection System (Bio-Rad, 1855201). *Gapdh* was used for normalization. Student's t-test was performed based on the  $\Delta\Delta C_T$  values. Unless otherwise specified, n=3 biological replicates per group were used for all qRT-PCR experiments. Primers were purchased from Eurofins Genomics. Primer sequences are listed in [Supplementary Table 1](#).

### Western blot

Cell and tissue samples were lysed in RIPA buffer containing protease inhibitor (Bimake, B14012) and phosphatase inhibitor (Bimake, B15002). Protein concentration was determined using the Pierce BCA Protein Assay Kit (Thermo Scientific, 23225). After determining concentration, 30 $\mu$ g of protein lysate was boiled at 95°C for 5 minutes in Laemmli buffer (Bio-Rad, 161-0747), and subsequently run on SDS-PAGE. Gels were transferred to PDVF membranes (Bio-Rad, 1620177) using the Bio-Rad Trans-Blot Turbo Transfer System. After transfer, membranes were blocked for 1 hour in 5% fat free milk in TBS-T. After blocking, membranes were incubated in primary antibodies at concentrations according to manufacturer specifications for either 2 hours at room temperature or 16 hours at 4°C, washed three times in TBS-T, incubated for 1 hour at room temperature with HRP-linked secondary antibody (Cell Signaling Technologies,  $\alpha$ Rabbit cat#7074,  $\alpha$ Mouse cat#7076), and then washed again three times in TBS-T. Subsequently membranes were imaged using Clarity ECL (Bio-Rad, 1705060) on the ChemiDoc XRS+ imager (Bio-Rad, 1708265). The antibodies used are listed in [Supplementary Table 2](#).

## Flow cytometry

Tumors were minced and digested in DMEM with 10% FBS and 1 mg/ml collagenase IV (STEMCELL Technologies, 07427) at 37°C for 1 h, followed by passing through 40µm strainers. Erythrocytes were depleted *via* hypotonic lysis. Cells were treated with mouse Fc-shield anti-CD16/CD32 (Tonbo Biosciences, 70-0161) for 15 minutes, and stained with primary fluorophore-conjugated antibodies for 30 minutes. Cells were washed twice and resuspended in a buffer containing DAPI (viability dye) and analyzed on the Beckman Coulter Cytoflex S cytometer. The antibodies used are listed in [Supplementary Table 2](#).

## Immunohistochemistry

Tumors and livers/spleens were fixed in 10% neutral buffered formalin (VWR, 16004-128) for 24 hours and prepared as paraffin-embedded 5 µm sections. Antigen retrieval was performed using sodium citrate buffer (pH 6.0) at 95°C for 30 minutes followed by 115°C for 10 seconds. After antigen retrieval, endogenous peroxidase activity was blocked using 3% hydrogen peroxide for 10 minutes. Subsequently samples were blocked in 5% normal goat serum in TBS-T for 30 minutes and incubated with primary antibody anti-mouse CD8 (Cell Signaling Technology, 98941) or cleaved caspase 3 (Cell Signaling Technology, 9661) in a humidified chamber at 4°C for 16 hours. After washing, the VECTASTAIN Elite ABC-HRP Kit (Vector Laboratories, PK-6101) was used as secondary antibody and signal detection. Counterstain was performed using Mayer's hematoxylin for 30 seconds. Imaging was performed using a Leica Aperio scanscope with 20× objective. At least 6 biological replicates were counted to quantify tumor-infiltrating CD8<sup>+</sup> T cells or cleaved caspase 3 staining.

Hematoxylin and eosin stain (H&E)

Livers were fixed in 10% neutral buffered formalin for 24 hours and prepared as paraffin-embedded 5 µm sections. After rehydration, samples were stained for 8 minutes in Mayer's hematoxylin. Excess dye was washed off in water for 8 minutes. Samples were immersed in 95% ethanol and stained in Eosin Y 1% (VWR, 101432-132) for 3 minutes. Excess dye was washed off in 95% ethanol after which slides were dehydrated and coverslipped and imaged using the Aperio scanscope.

## Tumor growth and inhibitor treatments

Syngeneic prostate tumor cell lines Myc-CaP or PPS was injected subcutaneously into 6-week-old FVB/NJ males or C57BL/6J males, respectively. Syngeneic mammary tumor cell line PyMT-7160 was injected to the mammary fat pads of 6-

week-old FVB/NJ females. Tumors were measured with calipers and volumes were calculated using the formula  $\text{length} \times \text{width}^2 \div 2$ . Mice with tumors reaching the pre-specified volume range were randomized to receive the following therapies: anti-PD-1 (clone RMP1-14, Leinco Technologies, P362) and anti-CTLA4 (clone 9H10, Leinco Technologies, C1614) were injected intraperitoneally at 10mg/kg, twice per week; NDNB1182 or Ganetespib was dissolved in 10% DMSO, 40% polyethylene glycol 300, 5% Tween-80 and 55% ddH<sub>2</sub>O and injected intraperitoneally at 50mg/kg and 25mg/kg daily, respectively. To select the dosage of NDNB1182 for animal experiments, a maximum tolerated dose (MTD) pilot experiment was conducted in five 10-week old FVB/NJ mice with escalated dosages. After 10 days of daily treatment, the dose of 50mg/kg was the highest dose that caused no significant body weight loss or body condition deterioration, thus this dose was defined in our study as the desired dose to administer NDNB1182 in mice. For Ganetespib, 25mg/kg daily was used based on previous reports (69, 70). All treatments were continued until the specified experimental endpoints were reached.

## Statistical analyses

Statistical analyses were performed using GraphPad Prism v8.0. Unless otherwise mentioned, all data were presented as mean ± SEM (standard error of the mean). Sample sizes, error bars, P values, and statistical methods were denoted in the figures or figure legends. Statistical significance was defined as  $P < 0.05$ .

## Data availability statement

The original contributions presented in the study are included in the article/[Supplementary Material](#). Further inquiries can be directed to the corresponding author.

## Ethics statement

The animal study was reviewed and approved by Institutional Animal Care and Use Committee at University of Notre Dame.

## Author contributions

SR: Conceptualization, investigation, methodology, data curation, formal analysis, validation, visualization, funding acquisition, writing – original draft. SJM: Resources. SM: Investigation. BB: Supervision. XL: Conceptualization, formal analysis, visualization, supervision, project administration,

funding acquisition, writing – original draft, writing – review & editing. All authors contributed to the article and approved the submitted version.

## Funding

SR was supported by an Interdisciplinary Interface Training Program Grant from the Walther Cancer Foundation and Harper Cancer Research Institute at University of Notre Dame. XL was supported by National Institutes of Health grant R01CA248033, Department of Defense CDMRP PCRP grants W81XWH2010312 and W81XWH2010332, and Boler Family Foundation endowment at University of Notre Dame.

## Acknowledgments

We would like to thank the Lu lab members for constructive suggestions. We are grateful for the support from core facilities used in this study, especially Freimann Life Science Center and Tissue Repository at Harper Cancer Research Institute.

## References

1. Waldman AD, Fritz JM, Lenardo MJ. A guide to cancer immunotherapy: from T cell basic science to clinical practice. *Nat Rev Immunol* (2020) 20(11):651–68. doi: 10.1038/s41577-020-0306-5
2. Sung H, Ferlay J, Siegel RL, Laversanne M, Soerjomataram I, Jemal A, et al. Global cancer statistics 2020: GLOBOCAN estimates of incidence and mortality worldwide for 36 cancers in 185 countries. *CA Cancer J Clin* (2021). doi: 10.3322/caac.21660
3. Topalian SL, Hodi FS, Brahmer JR, Gettinger SN, Smith DC, McDermott DF, et al. Safety, activity, and immune correlates of anti-PD-1 antibody in cancer. *New Engl J Med* (2012) 366(26):2443–54. doi: 10.1056/NEJMoa1200690
4. Kwon ED, Drake CG, Scher HI, Fizazi K, Bossi A, van den Eertwegh AJM, et al. Ipilimumab versus placebo after radiotherapy in patients with metastatic castration-resistant prostate cancer that had progressed after docetaxel chemotherapy (CA184-043): a multicentre, randomised, double-blind, phase 3 trial. *Lancet Oncol* (2014) 15(7):700–12. doi: 10.1016/S1470-2045(14)70189-5
5. Beer TM, Kwon ED, Drake CG, Fizazi K, Logothetis C, Gravis G, et al. Randomized, double-blind, phase III trial of ipilimumab versus placebo in asymptomatic or minimally symptomatic patients with metastatic chemotherapy-naive castration-resistant prostate cancer. *J Clin Oncol* (2017) 35(1):40–7. doi: 10.1200/jco.2016.69.1584
6. Antonarakis ES, Piulats JM, Gross-Goupil M, Goh J, Ojamaa K, Hoimes CJ, et al. Pembrolizumab for treatment-refractory metastatic castration-resistant prostate cancer: Multicohort, open-label phase II KEYNOTE-199 study. *J Clin Oncol* (2020) 38(5):395–405. doi: 10.1200/jco.19.01638
7. Sharma P, Pachynski RK, Narayan V, Fléchon A, Gravis G, Galsky MD, et al. Nivolumab plus ipilimumab for metastatic castration-resistant prostate cancer: preliminary analysis of patients in the CheckMate 650 trial. *Cancer Cell* (2020) 38(4):489–99:e483. doi: 10.1016/j.ccell.2020.08.007
8. Schmid P, Adams S, Rugo HS, Schneeweiss A, Barrios CH, Iwata H, et al. Atezolizumab and nab-paclitaxel in advanced triple-negative breast cancer. *N Engl J Med* (2018) 379(22):2108–21. doi: 10.1056/NEJMoa1809615
9. Cortes J, Cescon DW, Rugo HS, Nowecki Z, Im SA, Yusoff MM, et al. Pembrolizumab plus chemotherapy versus placebo plus chemotherapy for previously untreated locally recurrent inoperable or metastatic triple-negative breast cancer (KEYNOTE-355): a randomised, placebo-controlled, double-blind,

## Conflict of interest

The authors declare that the research was conducted in the absence of any commercial or financial relationships that could be construed as a potential conflict of interest.

## Publisher's note

All claims expressed in this article are solely those of the authors and do not necessarily represent those of their affiliated organizations, or those of the publisher, the editors and the reviewers. Any product that may be evaluated in this article, or claim that may be made by its manufacturer, is not guaranteed or endorsed by the publisher.

## Supplementary material

The Supplementary Material for this article can be found online at: <https://www.frontiersin.org/articles/10.3389/fimmu.2022.1005045/full#supplementary-material>

10. Whitesell L, Lindquist SL. HSP90 and the chaperoning of cancer. *Nat Rev Cancer* (2005) 5:761–72. doi: 10.1038/nrc1716
11. Taipale M, Jarosz DF, Lindquist S. HSP90 at the hub of protein homeostasis: Emerging mechanistic insights. *Nat Rev Mol Cell Biol* (2010) 11(7):515–28. doi: 10.1038/nrm2918
12. Schopf FH, Biebl MM, Buchner J. The HSP90 chaperone machinery. *Nat Rev Mol Cell Biol* (2017) 18(6):345–60. doi: 10.1038/nrm.2017.20
13. Jaeger AM, Whitesell L. HSP90: enabler of cancer adaptation. *Annu Rev Cancer Biol* (2019) 3:275–97. doi: 10.1146/annurev-cancerbio-030518-055533
14. Kamal A, Thao L, Sensintaffar J, Zhang L, Boehm MF, Fritz LC, Burrows FJ. A high-affinity conformation of Hsp90 confers tumour selectivity on Hsp90 inhibitors. *Nature* (2003) 425:407–10. doi: 10.1038/nature01913
15. Chiosis G, Neckers L. Tumor selectivity of Hsp90 inhibitors: the explanation remains elusive. *ACS Chem Biol* (2006) 1(5):279–84. doi: 10.1021/cb600224w
16. Trepel J, Mollapour M, Giaccone G, Neckers L. Targeting the dynamic HSP90 complex in cancer. *Nat Rev Cancer* (2010) 10(8):537–49. doi: 10.1038/nrc2887
17. Rodina A, Wang T, Yan P, Gomes ED, Dunphy MPS, Pillarsetty N, et al. The epichaperome is an integrated chaperome network that facilitates tumour survival. *Nature* (2016) 538(7625):397–401. doi: 10.1038/nature19807
18. Eustace BK, Sakurai T, Stewart JK, Yimlamai D, Unger C, Zehetmeier C, et al. Functional proteomic screens reveal an essential extracellular role for hsp90 alpha in cancer cell invasiveness. *Nat Cell Biol* (2004) 6(6):507–14. doi: 10.1038/ncb1131
19. Sidera K, Patsavoudi E. Extracellular HSP90: conquering the cell surface. *Cell Cycle* (2008) 7(11):1564–8. doi: 10.4161/cc.7.11.6054
20. Tsutsumi S, Scroggins B, Koga F, Lee MJ, Trepel J, Felts S, et al. A small molecule cell-impermeant Hsp90 antagonist inhibits tumor cell motility and invasion. *Oncogene* (2008) 27(17):2478–87. doi: 10.1038/sj.onc.1210897
21. Vilenchik M, Solit D, Basso A, Huezio H, Lucas B, He H, et al. Targeting wide-range oncogenic transformation via PU24FC1, a specific inhibitor of tumor Hsp90. *Chem Biol* (2004) 11(6):787–97. doi: 10.1016/j.chembiol.2004.04.008

22. Eiseman JL, Lan J, Lagattuta TF, Hamburger DR, Joseph E, Covey JM, et al. Pharmacokinetics and pharmacodynamics of 17-demethoxy 17-[(2-dimethylamino)ethyl]amino]geldanamycin (17DMAG, NSC 707545) in C.B-17 SCID mice bearing MDA-MB-231 human breast cancer xenografts. *Cancer Chemother Pharmacol* (2005) 55(1):21–32. doi: 10.1007/s00280-004-0865-3
23. Daozhen C, Lu L, Min Y, Xinyu J, Ying H. Synthesis of <sup>131</sup>I-labeled-[(131)I]iodo-17-allylamino-17-demethoxy geldanamycin ([<sup>131</sup>I]iodo-17-AAG) and its biodistribution in mice. *Cancer Biother. Radiopharm.* (2007) 22(5):607–12. doi: 10.1089/cbr.2006.363
24. Azad AA, Zoubeidi A, Gleave ME, Chi KN. Targeting heat shock proteins in metastatic castration-resistant prostate cancer. *Nat Rev Urol* (2015) 12(1):26–36. doi: 10.1038/nrurol.2014.320
25. Birbo B, Madu EE, Madu CO, Jain A, Lu Y. Role of HSP90 in cancer. *Int J Mol Sci* (2021) 22(19):10317. doi: 10.3390/ijms221910317
26. Whitesell L, Mimnaugh EG, De Costa B, Myers CE, Neckers LM. Inhibition of heat shock protein HSP90-pp60v-src heteroprotein complex formation by benzoquinone ansamycins: essential role for stress proteins in oncogenic transformation. *Proc Natl Acad Sci U.S.A.* (1994) 91(18):8324–8. doi: 10.1073/pnas.91.18.8324
27. Schulte TW, Akinaga S, Soga S, Sullivan W, Stensgard B, Toft D, et al. Antibiotic radicicol binds to the n-terminal domain of Hsp90 and shares important biologic activities with geldanamycin. *Cell Stress Chaperones* (1998) 3(2):100–8. doi: 10.1379/1466-1268(1998)003<0100:arbttn>2.3.co;2
28. Neckers L, Blagg B, Haystead T, Trepel JB, Whitesell L, Picard D. Methods to validate Hsp90 inhibitor specificity, to identify off-target effects, and to rethink approaches for further clinical development. *Cell Stress Chaperones* (2018) 23(4):467–82. doi: 10.1007/s12192-018-0877-2
29. Koren J3rd, Blagg BSJ. The right tool for the job: An overview of Hsp90 inhibitors. *Adv Exp Med Biol* (2020) 1243:135–46. doi: 10.1007/978-3-030-40204-4\_9
30. Sanchez J, Carter TR, Cohen MS, Blagg BSJ. Old and new approaches to target the Hsp90 chaperone. *Curr Cancer Drug Targets* (2020) 20(4):253–70. doi: 10.2174/1568009619666191202101330
31. Bagatell R, Paine-Murrieta GD, Taylor CW, Pulcini EJ, Akinaga S, Benjamin IJ, et al. Induction of a heat shock factor 1-dependent stress response alters the cytotoxic activity of hsp90-binding agents. *Clin Cancer Res* (2000) 6(8):3312–8.
32. Butler LM, Ferraldeschi R, Armstrong HK, Centenera MM, Workman P. Maximizing the therapeutic potential of HSP90 inhibitors. *Mol Cancer Res* (2015) 13(11):1445–51. doi: 10.1158/1541-7786.mcr-15-0234
33. Ficker E, Dennis AT, Wang L, Brown AM. Role of the cytosolic chaperones Hsp70 and Hsp90 in maturation of the cardiac potassium channel HERG. *Circ Res* (2003) 92(12):e87–100. doi: 10.1161/01.res.0000079028.31393.15
34. Peterson LB, Eskew JD, Vielhauer GA, Blagg BS. The hERG channel is dependent upon the Hsp90 $\alpha$  isoform for maturation and trafficking. *Mol Pharm* (2012) 9(6):1841–6. doi: 10.1021/mp300138n
35. Voss AK, Thomas T, Gruss P. Mice lacking HSP90beta fail to develop a placental labyrinth. *Development* (2000) 127(1):1–11. doi: 10.1242/dev.127.1.1
36. Grad I, Cederroth CR, Walicki J, Grey C, Barluenga S, Winssinger N, et al. The molecular chaperone Hsp90 $\alpha$  is required for meiotic progression of spermatocytes beyond pachytene in the mouse. *PLoS One* (2010) 5(12):e15770. doi: 10.1371/journal.pone.0015770
37. Duerfeldt AS, Peterson LB, Maynard JC, Ng CL, Eletto D, Ostrovsky O, et al. Development of a Grp94 inhibitor. *J Am Chem Soc* (2012) 134(23):9796–804. doi: 10.1021/ja303477g
38. Muth A, Crowley V, Khandelwal A, Mishra S, Zhao J, Hall J, et al. Development of radamide analogs as Grp94 inhibitors. *Bioorg. Med Chem* (2014) 22(15):4083–98. doi: 10.1016/j.bmc.2014.05.075
39. Crowley VM, Khandelwal A, Mishra S, Stothert AR, Huard DJ, Zhao J, et al. Development of glucose regulated protein 94-selective inhibitors based on the BnIm and radamide scaffold. *J Med Chem* (2016) 59(7):3471–88. doi: 10.1021/acs.jmedchem.6b00085
40. Crowley VM, Huard DJE, Lieberman RL, Blagg BSJ. Second generation Grp94-selective inhibitors provide opportunities for the inhibition of metastatic cancer. *Chemistry* (2017) 23(62):15775–82. doi: 10.1002/chem.201703398
41. Liu W, Vielhauer GA, Holzbeierlein JM, Zhao H, Ghosh S, Brown D, et al. KU675, a concomitant heat-shock protein inhibitor of Hsp90 and Hsc70 that manifests isoform selectivity for Hsp90 $\alpha$  in prostate cancer cells. *Mol Pharmacol* (2015) 88(1):121–30. doi: 10.1124/mol.114.097303
42. Mishra SJ, Khandelwal A, Banerjee M, Balch M, Peng S, Davis RE, et al. Selective inhibition of the Hsp90 $\alpha$  isoform. *Angew Chem Int Ed Engl* (2021) 60(19):10547–51. doi: 10.1002/anie.202015422
43. Khandelwal A, Kent CN, Balch M, Peng S, Mishra SJ, Deng J, et al. Structure-guided design of an Hsp90 $\beta$  n-terminal isoform-selective inhibitor. *Nat Commun* (2018) 9(1):425. doi: 10.1038/s41467-017-02013-1
44. Mishra SJ, Liu W, Beebe K, Banerjee M, Kent CN, Munthali V, et al. The development of Hsp90 $\beta$ -selective inhibitors to overcome detriments associated with pan-Hsp90 inhibition. *J Med Chem* (2021) 64(3):1545–57. doi: 10.1021/acs.jmedchem.0c01700
45. Mbofung RM, McKenzie JA, Malu S, Zhang M, Peng W, Liu C, et al. HSP90 inhibition enhances cancer immunotherapy by upregulating interferon response genes. *Nat Commun* (2017) 8(1):451. doi: 10.1038/s41467-017-00449-z
46. Zavareh RB, Spangenberg SH, Woods A, Martínez-Peña F, Lairson LL. HSP90 inhibition enhances cancer immunotherapy by modulating the surface expression of multiple immune checkpoint proteins. *Cell Chem Biol* (2021) 28(2):158–168.e155. doi: 10.1016/j.chembiol.2020.10.005
47. Subudhi SK, Vence L, Zhao H, Blando J, Yadav SS, Xiong Q, et al. Neoantigen responses, immune correlates, and favorable outcomes after ipilimumab treatment of patients with prostate cancer. *Sci Transl Med* (2020) 12(537):eaaz3577. doi: 10.1126/scitranslmed.aaz3577
48. Lániczky A, Gyórfi B. Web-based survival analysis tool tailored for medical research (KMplot): Development and implementation. *J Med Internet Res* (2021) 23(7):e27633. doi: 10.2196/27633
49. Kim J, Felts S, Llauger L, He H, Huezo H, Rosen N, et al. Development of a fluorescence polarization assay for the molecular chaperone Hsp90. *J Biomol. Screen* (2004) 9(5):375–81. doi: 10.1177/1087057104265995
50. Millson SH, Truman AW, Rác A, Hu B, Panaretou B, Nuttall J, et al. Expressed as the sole Hsp90 of yeast, the alpha and beta isoforms of human Hsp90 differ with regard to their capacities for activation of certain client proteins, whereas only Hsp90beta generates sensitivity to the Hsp90 inhibitor radicicol. *FEBS J* (2007) 274(17):4453–63. doi: 10.1111/j.1742-4658.2007.05974.x
51. Verba KA, Wang RY, Arakawa A, Liu Y, Shirouzu M, Yokoyama S, et al. Atomic structure of Hsp90-Cdc37-Cdk4 reveals that Hsp90 traps and stabilizes an unfolded kinase. *Science* (2016) 352(6293):1542–7. doi: 10.1126/science.aaf5023
52. Wu X, Yang X, Xiong Y, Li R, Ito T, Ahmed TA, et al. Distinct CDK6 complexes determine tumor cell response to CDK4/6 inhibitors and degraders. *Nat Cancer* (2021) 2(4):429–43. doi: 10.1038/s43018-021-00174-z
53. Goel S, DeCristo MJ, Watt AC, BrinJones H, Sceneay J, Li BB, et al. CDK4/6 inhibition triggers anti-tumour immunity. *Nature* (2017) 548(7668):471–5. doi: 10.1038/nature23465
54. Bock S, Mullins CS, Klar E, Pérot P, Maletzki C, Linnebacher M. Murine endogenous retroviruses are detectable in patient-derived xenografts but not in patient-individual cell lines of human colorectal cancer. *Front Microbiol* (2018) 9:789. doi: 10.3389/fmicb.2018.00789
55. Lu X, Horner JW, Paul E, Shang X, Troncoso P, Deng P, et al. Effective combinatorial immunotherapy for castration-resistant prostate cancer. *Nature* (2017) 543(7647):728–32. doi: 10.1038/nature21676
56. Attalla S, Taifour T, Bui T, Muller W. Insights from transgenic mouse models of PyMT-induced breast cancer: recapitulating human breast cancer progression in vivo. *Oncogene* (2021) 40(3):475–91. doi: 10.1038/s41388-020-01560-0
57. Watson PA, Ellwood-Yen K, King JC, Wongvipat J, Lebeau MM, Sawyers CL. Context-dependent hormone-refractory progression revealed through characterization of a novel murine prostate cancer cell line. *Cancer Res* (2005) 65(24):11565–71. doi: 10.1158/0008-5472.can-05-3441
58. Dudzinski SO, Cameron BD, Wang J, Rathmell JC, Giorgio TD, Kirschner AN. Combination immunotherapy and radiotherapy causes an abscopal treatment response in a mouse model of castration resistant prostate cancer. *J Immunother. Cancer* (2019) 7(1):218. doi: 10.1186/s40425-019-0704-z
59. Crowe AR, Yue W. Semi-quantitative determination of protein expression using immunohistochemistry staining and analysis: An integrated protocol. *Bio Protoc* (2019) 9(24):e3465. doi: 10.21769/BioProtoc.3465
60. Guan X, Polesso F, Wang C, Sehrawat A, Hawkins RM, Murray SE, et al. Androgen receptor activity in T cells limits checkpoint blockade efficacy. *Nature* (2022) 606(7915):791–6. doi: 10.1038/s41586-022-04522-6
61. Chiang N-J, Yeh K-H, Chiu C-F, Chen J-S, Yen C-C, Lee K-D, et al. Results of phase II trial of AUY922, a novel heat shock protein inhibitor in patients with metastatic gastrointestinal stromal tumor (GIST) and imatinib and sunitinib therapy. *J Clin Oncol* (2016) 34(4\_suppl):134–4. doi: 10.1200/jco.2016.34.4\_suppl.134
62. Graner MW. HSP90 and immune modulation in cancer. *Adv Cancer Res* (2016) 129:191–224. doi: 10.1016/bs.acr.2015.10.001
63. Graner MW. Making HSP90 inhibitors great again? unite for better cancer immunotherapy. *Cell Chem Biol* (2021) 28(2):118–20. doi: 10.1016/j.chembiol.2021.02.002
64. Hervouet E, Nadaradjane A, Gueguen M, Vallette FM, Cartron PF. Kinetics of DNA methylation inheritance by the Dnmt1-including complexes during the cell cycle. *Cell Div* (2012) 7:5. doi: 10.1186/1747-1028-7-5
65. Zivvogel L, Galluzzi L, Kepp O, Smyth MJ, Kroemer G. Type I interferons in anticancer immunity. *Nat Rev Immunol* (2015) 15(7):405–14. doi: 10.1038/nri3845

66. Yu R, Zhu B, Chen D. Type I interferon-mediated tumor immunity and its role in immunotherapy. *Cell Mol Life Sci* (2022) 79(3):191. doi: 10.1007/s00018-022-04219-z
67. Campbell IM, Gambin T, Dittwald P, Beck CR, Shuvarikov A, Hixson P, et al. Human endogenous retroviral elements promote genome instability via non-allelic homologous recombination. *BMC Biol* (2014) 12:74. doi: 10.1186/s12915-014-0074-4
68. Sheaffer KL, Elliott EN, Kaestner KH. DNA Hypomethylation contributes to genomic instability and intestinal cancer initiation. *Cancer Prev Res (Phila)* (2016) 9(7):534–46. doi: 10.1158/1940-6207.Ccr-15-0349
69. Lin TY, Bear M, Du Z, Foley KP, Ying W, Barsoum J, et al. The novel HSP90 inhibitor STA-9090 exhibits activity against kit-dependent and -independent malignant mast cell tumors. *Exp Hematol* (2008) 36(10):1266–77. doi: 10.1016/j.exphem.2008.05.001
70. Shimamura T, Perera SA, Foley KP, Sang J, Rodig SJ, Inoue T, et al. Ganetespib (STA-9090), a nongeldanamycin HSP90 inhibitor, has potent antitumor activity in *in vitro* and *in vivo* models of non-small cell lung cancer. *Clin Cancer Res* (2012) 18(18):4973–85. doi: 10.1158/1078-0432.Ccr-11-2967